Biochimica et Biophysica Acta 1787 (2009) 730–737

Contents lists available at ScienceDirect

Biochimica et Biophysica Acta

journal homepage: www.elsevier.com/locate/bbabio

Infrared spectroscopic study of the structural and functional properties of the Na^+/H^+ antiporter MjNhaP1 from *Methanococcus jannaschii*☆

E. Džafić [a], O. Klein [a], P. Goswami [b], W. Kühlbrandt [b], W. Mäntele [a,*]

[a] Institut für Biophysik, Johann Wolfgang Goethe-Universität, Max-von-Laue-Straße 1, 60438, Frankfurt am Main, Germany
[b] Max Planck Institute of Biophysics, Department of Structural Biology, Max-von-Laue-Straße 3, D-60438, Frankfurt am Main, Germany

ARTICLE INFO

Article history:
Received 6 February 2009
Received in revised form 2 April 2009
Accepted 2 April 2009
Available online 9 April 2009

Keywords:
Na^+/H^+ antiporter
M. jannaschii MjNhaP1
FTIR spectroscopy
Attenuated total reflection
ATR
Secondary structure analysis
H/D exchange
Protein accessibility
Temperature-induced structural changes

ABSTRACT

In this study, structural, functional, and mechanistic properties of the Na^+/H^+ antiporter MjNhaP1 from *Methanococcus jannaschii* were analyzed by infrared spectroscopic techniques. Na^+/H^+ antiporters are generally responsible for the regulation of cytoplasmic pH and Na^+ concentration. MjNhaP1 is active in the pH range between pH 6 and pH 6.5; below and above it is inactive. The secondary structure analysis on the basis of ATR-IR spectra provides the first insights into the structural changes between inactive (pH 8) and active (pH 6) state of MjNhaP1. It results in decreased ordered structural elements with increasing the pH-value i.e. with inactivation of the protein. Analysis of temperature-dependent FTIR spectra indicates that MjNhaP1 in the active state exhibits a much higher unfolding temperature in the spectral region assigned to α-helical segments. In contrast, the temperature-induced structural changes for β-sheet structure are similar for inactive and active state. Consequently, this structure element is not the part of the activation region of the protein. The surface accessibility of the protein was analyzed by following the extent of H/D exchange. Due to higher content of unordered structural elements a higher accessibility for amide protons is observed for the inactive as compared to the active state of MjNhaP1. Altogether, the results present the active state of MjNhaP1 as the state with ordered structural elements which exhibit high thermal stability and increased hydrophobicity.

1. Introduction

Na^+/H^+ antiporters are integral membrane proteins that play an important role in the maintenance of cytoplasmic pH optimum, sodium concentration and cellular volume [1–3]. They use an electrochemical gradient to drive the secondary active transport of protons and sodium in opposite directions. This ion transport is strictly controlled by pH involving pH-sensitive groups in order to detect the intracellular and extracellular concentrations. Protonation changes of a pH-sensor leads to conformational changes which induce the activity of the protein and consequently enable the transport of ions [2–4].

MjNhaP1 is a Na^+/H^+ antiporter from the hyperthermophilic archeon *Methanococcus jannaschii* [5]. Its sequence of 426-amino acids is folded into 12 or 13 transmembrane domains [6]. MjNhaP1 exhibits higher sequence homology to the mammalian antiporter NHE1 than to the best-characterized bacterial antiporter NhaA from *E. coli* [4,6,7]. In contrast to NhaA and similar to NHE1, MjNhaP1 is active in the pH range from 6 to 6.5 and is deactivated at pH values above pH 7 and below pH 6 [5,6]. At pH values below 5, it is thought to be in a "closed" conformation, while at pH values above 7 a "blocked" conformation has been proposed [8].

Based on the structure of the best-characterized antiporter NhaA in a down-regulated conformation, binding of charged substrates is proposed to induce conformational changes that provide alternating access from both sides [7,9,10]. The binding site for Na^+ is thought to be formed by residues Asp 164, Asp 163 and Thr 132. Exposure of these sites to either the cytoplasmic funnel or to the periplasm is part of proposed transport model, which involves conformational changes and/or changes in helix orientation. However, the precise mechanism of activation and transport are unclear.

In the present study we use infrared spectroscopy to characterize two different functional states of MjNhaP1, the active state at pH 6 and the inactive state at pH 8. The most prominent vibrational modes of the protein are reflected in the amide I and the amide II mode, respectively [11–13]. The amide I mode is mainly composed of the absorption of C=O stretching mode of polypeptide backbone and gives information about secondary structure components of the protein. The signal of the amide II mode results from coupled N–H bending and C N stretching vibrations. The structural changes between the inactive and the active state of MjNhaP1 are followed by analysis of the secondary structure using the amide I band profile in H_2O and D_2O buffer [13–16]. The use of temperature as an external perturbation is used to compare the stability of individual secondary structure elements for these two states

☆ This work was supported by the Deutsche Forschungsgemeinschaft (SFB 472 / P21).
* Corresponding author. Tel.: +49 69 798 46410; fax: +49 69 798 46423.
E-mail address: maentele@biophysik.uni-frankfurt.de (W. Mäntele).

0005-2728/$ – see front matter © 2009 Elsevier B.V. All rights reserved.
doi:10.1016/j.bbabio.2009.04.002

[17–19]. The surface accessibility, flexibility and dynamics of the protein in its inactive and active state was analyzed using H/D exchange monitored at the amide II mode [19–22].

2. Materials and methods

2.1. Preparation of MjNhaP1 Na^+/H^+ antiporter from Methanococcus jannaschii

The construct used for the expression of MjNhaP1 has been published earlier [8]. The protein expression was carried out by the method of autoinduction [23] in bacterial pLysS cells. Cultures grown at 37 °C were harvested after 16–18 h of growth. The previously described [8] protein purification protocol was adopted with few modifications. An additional step of 65 mM imidazole wash was introduced to the published protocol before finally eluting the protein with 300 mM imidazole. The eluted protein was dialysed for 2–3 h to 25 mM Na-Actetate pH 4.0, 10% glycerol, 300 mM NaCl, 2 mM beta Mercaptoethanol or 2–3 mM DTT and 0.05% n-Dodecyl β-D-maltoside (DDM, Glycon).

2.2. Secondary structure analysis of MjNhaP1 in H_2O and D_2O buffer

For a secondary structure analysis, spectra recorded in a FTIR-ATR microdialysis perfusion cell were used. This perfusion cell was developed using a diamond ATR unit with 7 reflections, for details see [19]. The target protein (5 µl, 1 mM) was kept in contact with the ATR crystal and separated from the continuous flow buffer by a dialysis membrane (molecular weight cut-off 25 kDa). The initial buffer for the protein was a sodium citrate buffer pH 4. Perfusion was started with a 66 mM H_2O potassium phosphate buffer (pH 6 for the active state and pH 8 for the inactive state of the antiporter, resp.) with 100 mM NaCl and 0.03% DDM. The protein spectra in H_2O buffer were taken 1 h after beginning of the perfusion to ensure that the initial citrate buffer was completely replaced. The second perfusion buffer was a D_2O buffer (pD 6 or pD 8). Switching from pH 6 to pD 6 initiates the process of H/D exchange of the protein. The spectra recorded after 24 h perfusion with the buffer at pD 8 or pD 6 are used for secondary structure analysis of the fully exchanged protein in D_2O buffer.

For the evaluation of the amide I band profiles, curve fitting was performed with the OPUS Software (Bruker Optics). Spectra were prepared by baseline correction for the amide I band using the minima at the low- and high-frequency sides. The number of component bands and their maxima in the amide I region were determined from the second and fourth derivative of the spectra. The result of the curve fits were controlled by a comparison of the second derivatives of the original and the fitted curve; only fits with matching secondary derivatives were accepted.

2.3. Thermal profiling of MjNhaP1

Temperature-induced conformational changes of MjNhaP1 were followed in the course of a temperature ramp. IR spectra were recorded on a Bruker Vektor 22 FTIR spectrometer equipped with a DTGS detector. For these experiments, the sodium citrate buffer pH 4 was replaced by a phosphate buffer containing10 mM NaCl and 0.03% DDM at pD 6 or pD 8, resp., using Microcon Centrifugal Filter Devices MWCO 30,000 Da (Millipore). The sample was placed in a thermostated IR cell equipped with Ca_2F windows at a path length of 10 µm [19]. The temperature ramp was started after equilibration of the samples at 10 °C. For each spectrum 128 scans with 4 cm^{-1} nominal resolution were taken. The temperature was increased stepwise from 10 to 90 °C in 2 °C intervals using a water bath controlled by the spectroscopy software.

2.4. H/D exchange of MjNhaP1 using an ATR microdialysis cell

A previously described ATR microdialysis perfusion cell [19] was used to follow the process of H/D exchange. Exchange was performed starting from an H_2O buffer (pH 8 for the inactive state; pH 6 for the active state) and leading to a D_2O buffer (pD 8 or pD 6, resp.). The protein sample in H_2O buffer was equilibrated by continuous flow of the phosphate buffer at pH 6 or pH 8 each containing 100 mM NaCl and 0.03% DDM. As soon as stable IR absorbance spectra were obtained, the H_2O buffer was exchanged by a continuous flow of D_2O buffer [24]. The volume of the circulating D_2O buffer was chosen big enough to ensure a high D_2O fraction in the total volume (>99%). After ~24 h at a given pD-value to ensure full equilibration, the pD-value was again switched (from pD 8 to 6 or reverse) to study activation/deactivation in D_2O buffers. The temperature of the ATR-perfusion system was regulated at 4 °C by a water bath. Spectra were recorded every 5 min with 256 scans at 2 cm^{-1} resolution.

For the analysis of the spectra, buffer spectra were first subtracted as described before in [19]. The ratio of the integrated amide II and

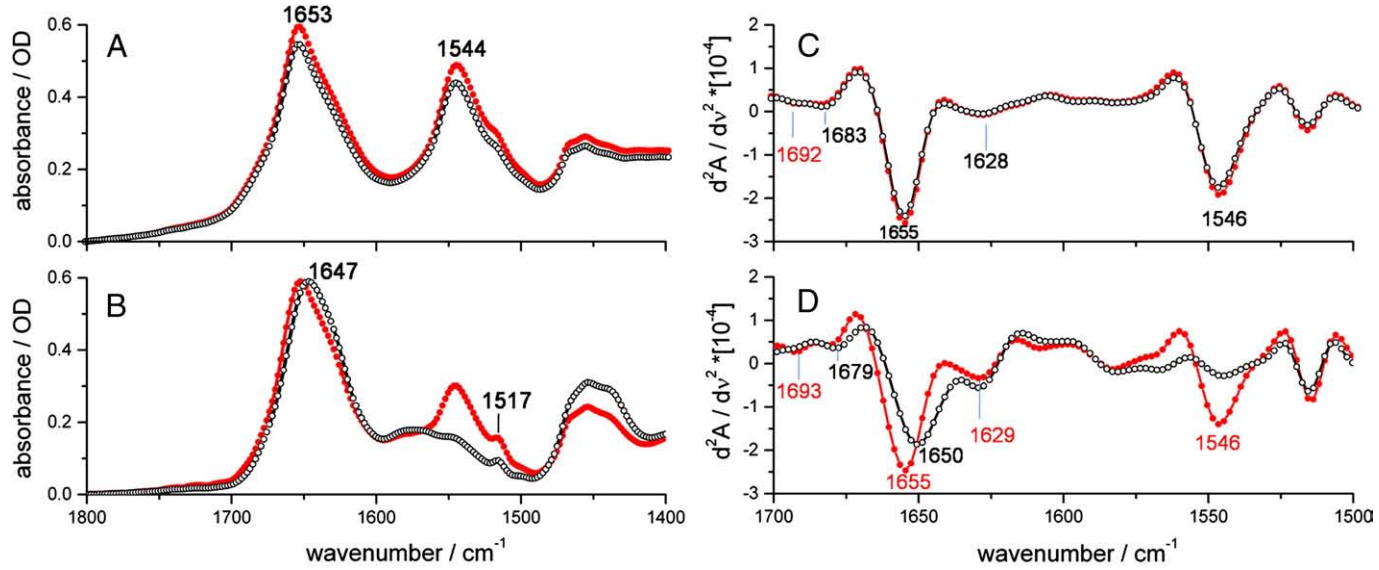

Fig. 1. ATR-IR absorbance spectra of MjNhaP1 (A) in H_2O and (B) in D_2O buffer at pH or pD 6 (●) and at pH or pD 8 (○). The second derivative (C) of the spectra shown in (A) and (D) the second derivative of the spectra shown in (B).

amide I band intensities was used to calculate the extent of H–D exchange in the protein.

3. Results

3.1. Secondary structure analysis of MjNhaP1 in H_2O and D_2O buffer

A critical point in amide I band based secondary structure analysis is the comparison of two samples prepared in H_2O and D_2O. The use of the ATR-perfusion method allowed us to analyse the spectra taken in H_2O and D_2O buffer from the same protein sample.

Fig. 1 shows the IR absorbance spectra in H_2O (Fig. 1A) and in D_2O (Fig. 1B) buffers together with the corresponding second derivative spectra in H_2O (Fig. 1C) and in D_2O (Fig. 1D). The active forms (pH 6, pD 6) and the inactive forms (pH8, pD 8) are shown together.

The absorbance spectrum in H_2O buffer (Fig. 1A) in the 1800–1400 cm^{-1} interval is mainly composed of 2 bands, the amide I centred at 1653 cm^{-1} and the amide II band at 1544 cm^{-1}. The amide I maximum is typical for membrane proteins with high α-helical content [13,16,25].

The second derivative spectra (Fig. 1C) indicate that the amide I band is dominated by a band appearing at 1655 cm^{-1}, which can be assigned mainly to α-helices with some possible contribution of unordered structural elements [12,13,26]. The band absorbing at 1628 cm^{-1} together with the bands at 1683 cm^{-1} and 1692 cm^{-1} indicates some extended configurations in the protein (including β-sheet structure) [17,27–29]. The amide I band at 1683 cm^{-1} could be also assigned to β-turns [17,25].

Figs. 1B and D show the spectra recorded from MjNhaP1 equilibrated for 24 h in D_2O buffer at pD 6 for the active and at pD 8 for the inactive state. As can be observed, the effect of H/D exchange is more pronounced for the inactive state of the protein at pD 8. The rate and extent of H-D exchange depends on protein accessibility, flexibility and dynamics. The strong decrease of the amide II band absorbance with maximum at 1547 cm^{-1} at pD 8 as compared to pD 6 can thus be taken as evidence for higher protein accessibility in the inactive state and will be discussed more in detail below.

In the amide I range, the peak positions essentially match for the active and the inactive form (Figs 1A, B) in H_2O. In contrast to this, a shift to lower wavenumbers is observed after H/D exchange for the inactive form (Fig. 1D). This indicates some structural difference in the α-helical parts between the inactive and active state of the protein. The shift to lower wavenumbers cannot be observed for extended structural elements absorbing at around 1629 cm^{-1}.

For secondary structure quantification of MjNhaP1 in the inactive and the active state, curve fitting procedures for the amide I band profile were applied. Fig. 2 shows the amide I spectrum of MjNhaP1 in H_2O (pH 6, active form: Fig. 2A and pH 8, inactive form Fig. 2B) and in D_2O buffer (pD 6, active form: Fig. 2C and pD 8, inactive form Fig. 2D) with a fit from its component bands. Band positions and areas are listed in Table 1. In addition, the assignment proposed for each band component is given. The assignment of the band absorbing at around 1640 cm^{-1} in H_2O and D_2O buffer is not unambiguous, because other structures gives also rise to bands in this spectral region such as 3_{10}-helix or coupled helical structures [30,31]. Based on these results, the secondary structure of MjNhaP1 in the active state pH or pD 6 is composed of ~14% turns, ~50% α-helices and ~35% extended configurations.

In contrast to the active state a big difference is observed between samples in H_2O and D_2O buffer in the inactive state (pH/pD 8) of the protein. This may be explained by the strong overlap of the amide I component arising from unordered structural elements with that from α-helices in H_2O buffer [11,13]. In contrast to that, the amide I component from unordered structure shifts to lower wavenumbers in D_2O buffer, much stronger (~1642 cm^{-1}) as compared to that from α-helices (~1652 cm^{-1}).

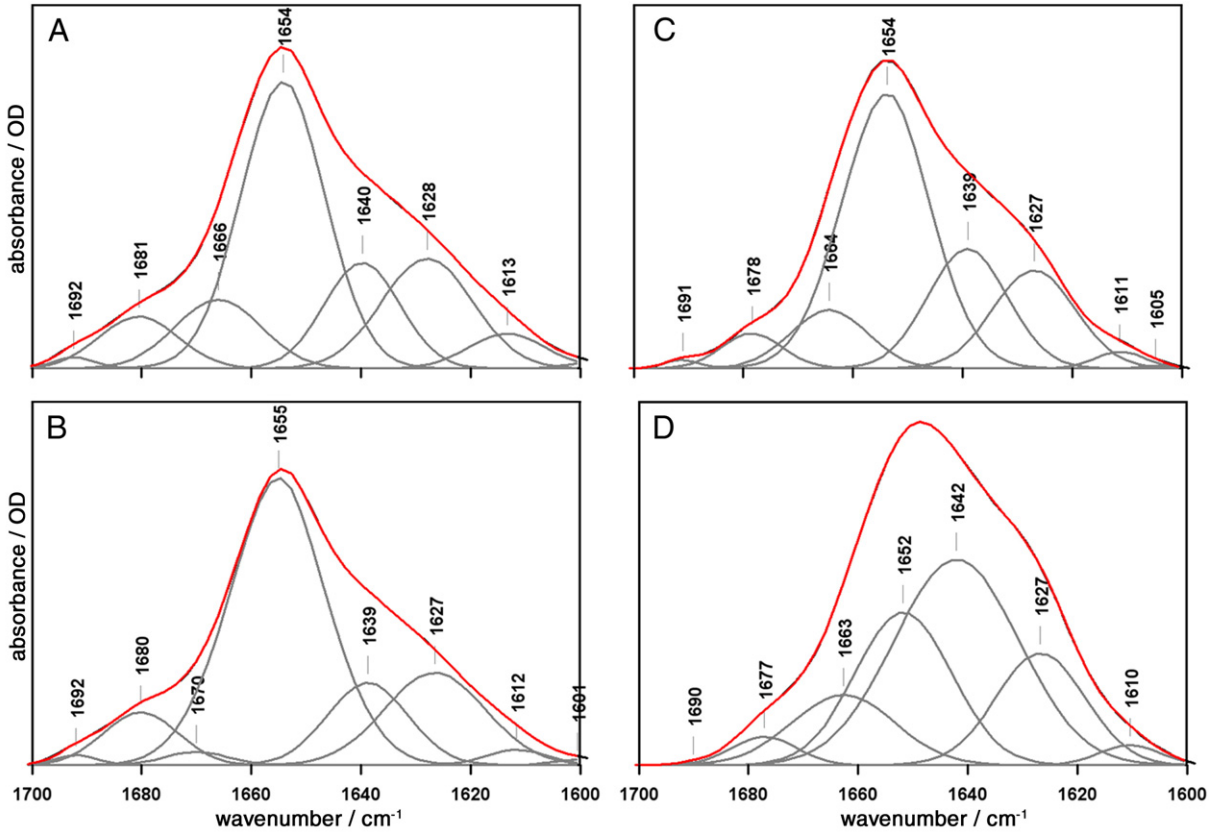

Fig. 2. Amide I spectra of MjNhaP1 and the component bands used for band synthesis (A) pH 6, (B) pH 8, (C) pD 6 and (D) pD 8.

Table 1
Secondary structure composition and assignments for active (pH/pD 6) and inactive (pH/pD 8) state of MjNhaP1.

H_2O					D_2O				
pH 6 (active) ν/cm^{-1}	% area	pD 8 (inactive) ν/cm^{-1}	% area	Assignment	pD 6 (active) ν/cm^{-1}	% area	pD 8 (inactive) ν/cm^{-1}	% area	Assignment
1692	1	1692	1	Turns	1691	1			Turns
1681	7	1680	8		1678	4	1677	3	
1666	11	1670	2		1664	9	1663	12	
1655	43	1655	56	α, unordered	1654	49	1652	24	α
							1642	42	Unordered, β
1640	14	1639	13	α, β, extended	1639	19			α, β, extended
1628	18	1627	19	β, extended	1627	16	1627	16	β, extended
1613	5	1612	2	Side chains	1611	2	1610	2	Side chains

This difference in the sensitivity to H/D exchange allows a separation of the amide components involved. At pH 8, the band at 1655 cm^{-1} accounts for approx. 56% of the amide I signal, while at pD 8 this amount is decreased to approx. 24%. Consequently, about 30% of secondary structure absorbing at 1642 cm^{-1} is disordered in the inactive state, representing the major difference in the secondary structure composition between these two states.

The residual amount of the band at 1642 cm^{-1} is probably caused by absorbance of the band at 1639 cm^{-1} that is also seen in H_2O buffer and assigned to extended structure including β-sheet and open loops.

The band at ~1627 cm^{-1} is observed in H_2O as well as in D_2O buffer and apparently independent from state of the protein. Bands in this wavenumber range can be assigned reliably to intermolecular β-sheet caused for example by intermolecular hydrogen bonding in the course of monomer monomer interaction [27,32]. This band thus indicates the existence of MjNhaP1 as an oligomeric protein and supports the result from blue native gel which shows that MjNhaP1 exists as dimer [8]. Gel filtration profiles of MjNhaP1 in DDM buffer at pH 4.0 and pH 8.0 has the same retention volume which allows the conclusion of dimeric MjNhaP1.

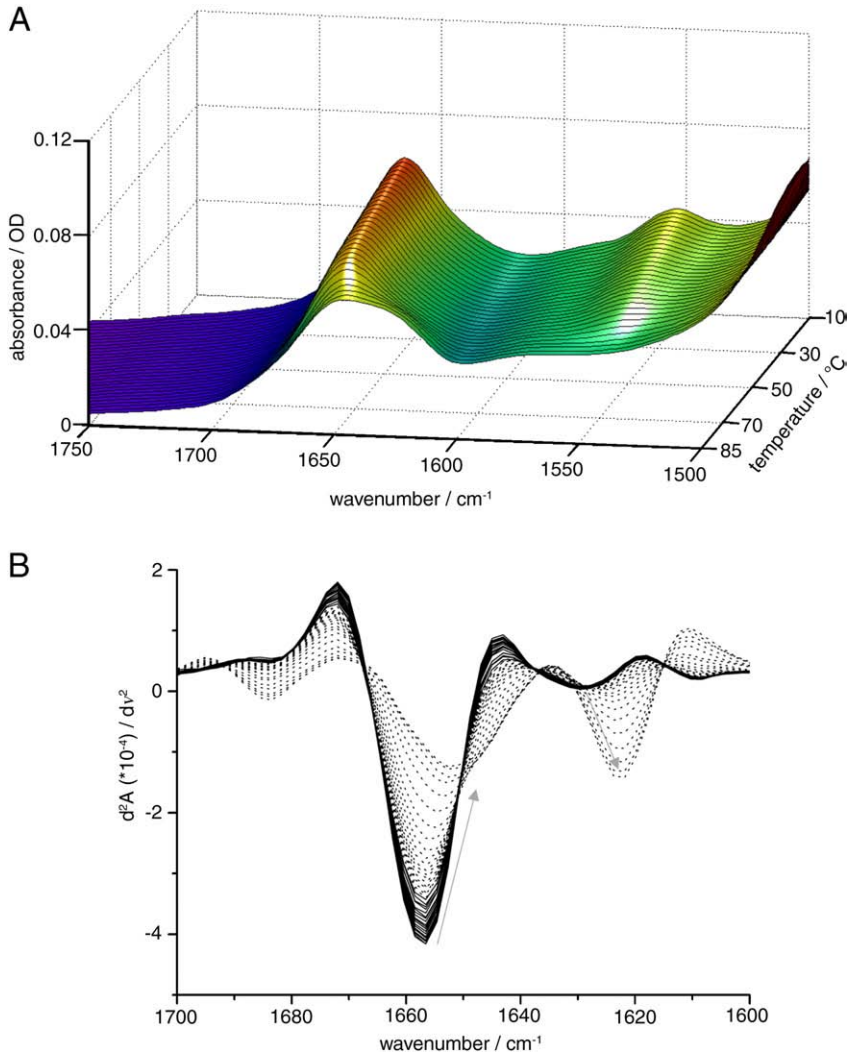

Fig. 3. Temperature profiling of MjNhaP1 at pD 6. (A) 3D-plot of temperature-induced FTIR absorbance spectra between 10 °C and 95 °C for the amide I and amide II range. (B) Second-derivative of the amide I band shown in (A). The solid lines represent the second derivative of the spectra taken in the range between 10 °C and 50 °C and dashed lines, of that taken between 50 °C and 85 °C. The arrows indicate the shift of α-helical band at 1657 cm^{-1} and of the β-sheet band at 1629 cm^{-1} with temperature.

The protein bands at frequencies <1615 cm^{-1} are more likely due to absorbance of amino acid side chains like Tyr-OH, Asn and/or Tyr [33].

However, the result of secondary structure analysis with FTIR-spectroscopy shows that the main difference between MjNhaP1 at pH/pD 6 and MjNhaP1 at pH/pD 8 is a different content of α-helical structure. With increasing of pH-value the decrease of ordered structural elements such α-helix is observed. Similar results were also obtained from secondary structure analysis with CD-spectroscopy (data not shown).

3.2. Temperature-induced conformational changes

In the inactive state at pD 8, the secondary structure analysis results in a high amount of disordered structural elements. According to this result, the thermal stability of the protein at pD 6 should be much higher than at pD 8 because of higher content of ordered structure at this pD-value. In order to verify this assumption, the conformational change of MjNhaP1 as a function of temperature was studied at pD 6 and pD 8.

Figure 3A shows the absorbance spectra of MjNhaP1 at pD 6 as a function of temperature. The amide I band intensity decreases and a new component at lower wavenumbers increases with rising temperature. The amide II intensity diminishes, indicating an increase of deuteration and a loss of tertiary structure with higher temperature. This increased deuteration is the consequence of a more flexible and dynamic conformation at elevated temperature. To resolve the amide I band into its components, the second derivative was calculated (Fig. 3B).

The second derivative profile of the amide I region indicates three main minima. At 10 °C the band at 1629 cm^{-1} indicates the presence of β-sheet, while the band at 1657 cm^{-1} indicates the presence of α-helices. As the temperature increases, the band for α-helices decreases and shifts to lower wavenumbers (approx. 1652 cm^{-1}). A shift to lower wavenumbers (approx. 1623 cm^{-1}) can also be observed for β-sheet. In contrast to the α-helical components, the intensity of this component rises with temperature. The spectrum at 85 °C shows the typical pattern of a thermally denatured protein with prominent bands at around 1684 and 1623 cm^{-1}, indicating the formation of aggregation β-sheet [34–36]. The temperature-dependent denaturation of MjNhaP1 is irreversible (not shown). The transition temperature of all samples was followed individually for α-helices and β-sheet components, using second derivative spectra, by following the degree of shift with respect to temperature. A sigmoidal fit to the data points (Fig. 4) was performed using ORIGIN software.

In these diagrams, we can distinguish conformational changes of protein in three temperature regions. The first region (for example,

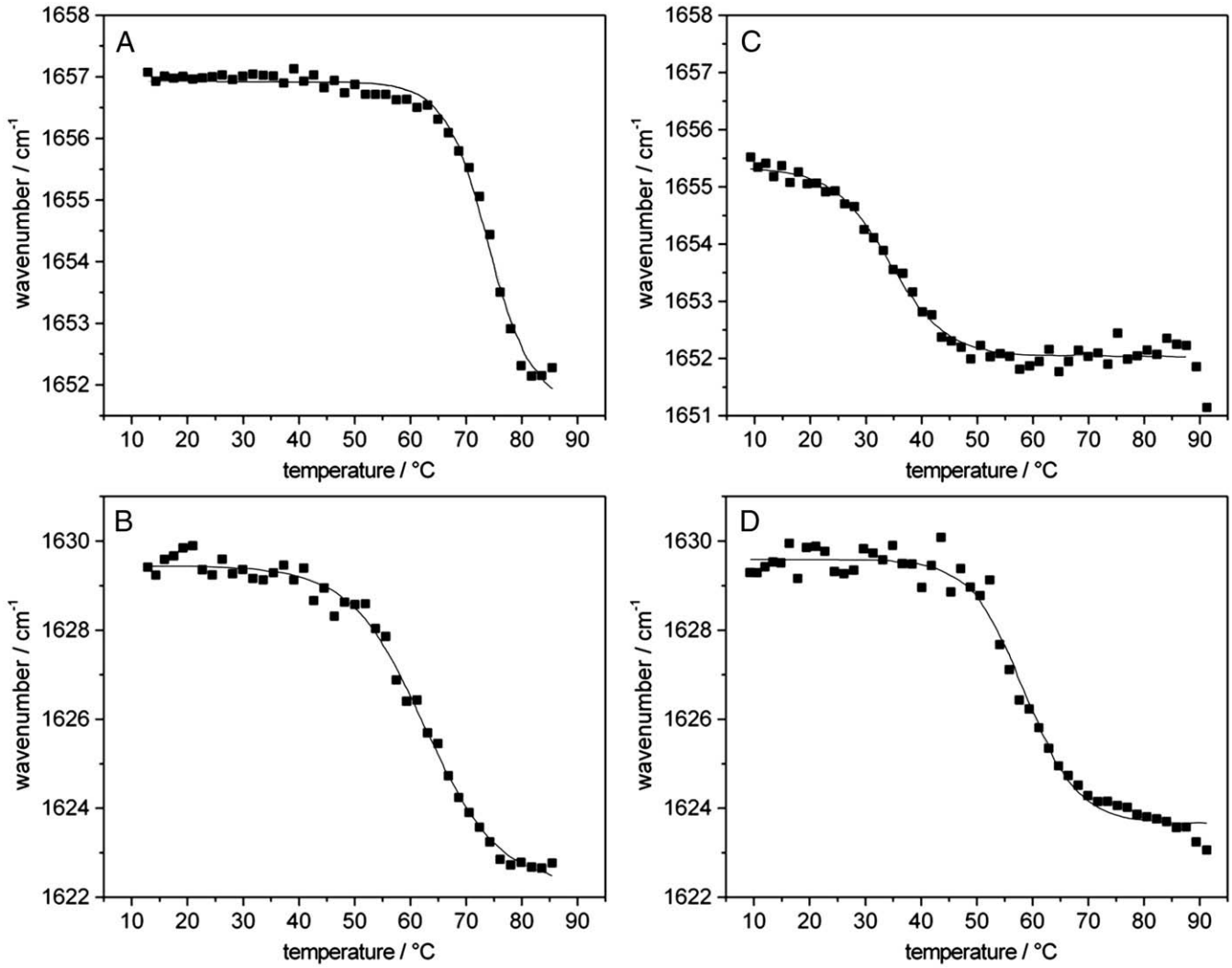

Fig. 4. Thermal profiles of MjNhaP1 for inactive and active state for α-helix and β-sheet components. The solid lines represent a sigmoidal fit used for determination of T_M (melting temperature): (A) α-helix at pD 6 with $T_M = 74$ °C, (B) β-sheet at pD 6 with $T_M = 62$ °C, (C) α-helix at pD 8 with $T_M = 34$ °C and (D) β-sheet at pD 8 with $T_M = 58$ °C.

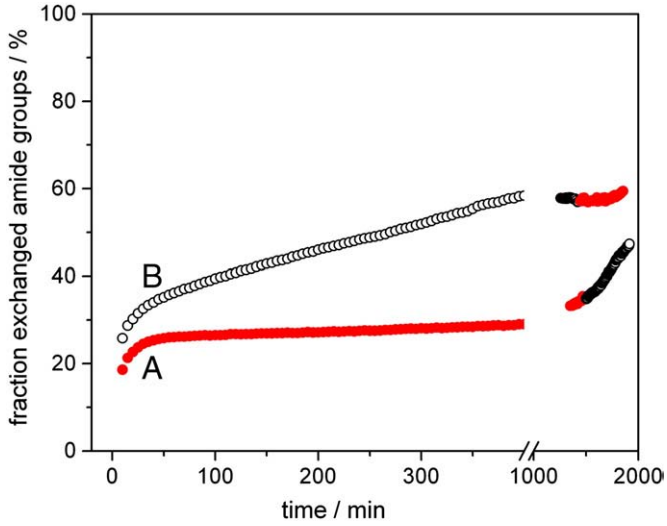

Fig. 5. Monitoring of H/D exchange as a function of the deuteration time by using amide II/amide I ratio: (A) for the active state (●) at pH/pD 6 and change after ~24 h to pD 8 (○) (B) for the inactive state (○) at pH/pD 8 and change after ~24 h to pD 6 (●).

between 10 °C and ~60 °C in Fig. 4A) describes the protein in the native state and no conformational changes can be observed with the temperature. The second region (for example, between ~60 °C and ~80 °C in Fig. 4A) begins with the temperature-induced structural changes and ends with third region in which the protein is fully denaturated.

Before these temperature profiles were started, the protein samples were equilibrated for the same time in D_2O buffer to ensure a comparable H/D exchange.

However, at 10 °C the protein sample in the inactive state at pD 8 shows a component of α-helix which is shifted by about 1.5 cm^{-1} to lower wavenumbers (1655.5 cm^{-1}). This supports the result of secondary structure analysis of higher content of unordered structural elements at pD 8 because peptide groups from unordered structure are faster accessible for solution and will perform H/D considerably faster than those in ordered structural elements.

The inactivation of the protein at pD 8 causes a state of the protein with highly reduced thermal stability as compared to the active state (pD 6). In detail, the unfolding process, i.e. the second range in the thermal profile at pD 8 starts already at about 20 °C while it is not observed at temperatures up to 65 °C at pD 6. At pD 8, this process is completed at around 50 °C with a melting temperature of 34 °C and at pD 6 at approx. 85 °C with a melting temperature of 74 °C. The huge difference in thermal stability of 40 °C between the inactive and the active state of the protein cannot be explained through minor structural differences, but rather through substantial conformational changes between these two states of the protein which were already suggested in Table 1.

At pD 6 and pD 8, the band related to α-helical structures absorbs at different positions at 10 °C. In contrast to that, the position related to the β-sheet components (1629 cm^{-1}) is the same at pD 6 as well as pD 8. In both states of the protein, the unfolding process of these structure elements begins at approximately 45 °C. The melting temperature amounts to around 60 °C with a difference of 4 °C between pD 6 and pD 8. Finally, the third region is characterized by formation of intermolecular β-sheet at ~1623 cm^{-1}.

3.3. H/D exchange of MjNhaP1

Information about flexibility and dynamics of the protein can be obtained from the accessibility of the protein backbone groups through H/D exchange experiments. The rate and extent of H/D exchange is monitored at the using amide II band [20,22,28,37,38]. The IR spectrum of the protein in H_2O buffer is characterized the by amide II band which extends over a region from 1600 cm^{-1} to 1500 cm^{-1} with its absorption maximum at 1544 cm^{-1} in the case of MjNhaP1. This band is mainly due to N–H bending (~60%) and C–N–H stretching vibration (~40%) with some contribution of C–C stretching vibration of the peptide group [20].

The substitution of H_2O buffer through D_2O buffer results in the gradual substitution of N–H by N–D bending vibrations for accessible amide modes. This substitution causes the amide II mode to disappear and a new mode, amide II', to appear at approx 1500–1400 cm^{-1}. The rate and extend of this exchange depend on global accessibility of the respective protein domains for water and finally the local accessibility. This accessibility of MjNhaP1 was calculated on the basis of the amide II band amplitudes (or areas) for the inactive and the active state, respectively. The amide II band was integrated between 1600 and 1500 cm^{-1} and normalized with respect to the amide I band, by division of the amide II band by the integrated amide I band (1700–1600 cm^{-1}).

H/D exchange of MjNhaP1 was monitored in two different experiments. In one experiment H/D exchange was followed first for the active state (pH 6/pD 6) of MjNhaP1 for a period of 24 h. Upon increasing the pD-value to pD 8, the protein was brought into the inactive state, allowing to study the exchange rate with inactivation of the protein. In the second experiment the reverse procedure was performed. Fig. 5 shows the accessible fraction of the polypeptide chain of MjNhaP1 obtained by two different experiments. As can be observed in first parts of two experiments, the increase of pD-value is accompanied by an increase of H/D exchange. After approximately 10 min approx. 19% of amide groups were accessible at pH/pD 6 (Fig. 5A). This fraction increased to approx. 26% at pH/pD 8 (Fig. 5B). The amide hydrogen exchange rise dramatically with pD 8 and reaches 58% after 400 min, while at pD 6 an increase of only about 3% is observed. At the end of first parts of the two experiments after approximately 24 h, the inactive protein (pD 8) does not show further exchange. In contrast, additional approx. 6% exchange of amide hydrogens are observed in the active state of the protein (pD 6), indicating the slowly exchanging part of the protein.

In the second part of two experiments, the pD-values were changed. By increasing the pD-value from pD 6 to pD 8 (Fig. 5A) as expected, the increase of H/D exchange is observed. The fraction of exchanged amide groups remains constant by lowering the pD-value from pD 8 to pD 6 (Fig. 5B).

The results of H/D exchange experiments indicate the conformation of the protein at pD 8 which is easily accessible for solution. However, the high H/D exchange at inactive state is observed just in the first 400 min. This result confirms the high amount of unordered structure observed with secondary structure analysis as well as high thermal instability of inactive protein (pD 8) in comparison to active protein (pD 6).

4. Discussion

In the present study infrared spectroscopic techniques were used to characterize the conformational alterations in MjNhaP1 from *Methanococcus jannaschii* upon activation/inactivation induced by pH.

The IR spectrum of MjNhaP1 with amide I band at 1653 cm^{-1} and amide II band at 1544 cm^{-1} is representative for proteins with high α-helical content [13,16,25,39]. In comparison with the IR absorption spectrum of the Na^+/H^+ antiporter NhaA from *Escherichia coli*, the position of the amide I and amide II maxima are shifted to lower wavenumbers for MjNhaP1 [19]. This indicates a different intermolecular interaction or varieties of the arrangement of α-helical segments in these two proteins. The position of the amide I band of NhaA band at 1658 cm^{-1} points to α-helices which are more flexible and dynamic than the standard α-helices that are probably related to the amide I band at 1653 cm^{-1}, which is found for MjNhaP1 [25,40].

The result of the secondary structure analysis shows that this membrane protein in the active state (pH/pD 6) predominantly adopts an α-helical structure, although some turns and extended structures including β-sheet are also present. The band absorbing at approx. 1640 cm^{-1} in H_2O and in D_2O buffer cannot be unambiguously assigned because β-sheet as well as α-helix can contribute to signals in this region [30,31,40]. This band accounts for about 15% of the secondary structure of the protein. Considering that the α-helical structure absorbing at ~1655 cm^{-1} constitutes to 50%, total α-helical contribution to the protein structure is about 65% in the active state. These probably present the transmembrane segments of the protein.

This result was also supported by the results of H/D exchange experiments, which show MjNhaP1 in the active state as much less accessible, giving rise to an exchange of only 35% of the amide protons. These results are in very good agreement with results of the model deduced from the amino acid sequence [6], which proposed that the polypeptide chain crosses the membrane 13 times with 21 amino acid residues each, accounting for about 64% of the 426 amino acid residues of the protein.

Our FTIR secondary structure analysis has also revealed a presence of β-sheet structure for MjNhaP1, quite similar to the analysis of NhaA from *Escherichia coli* [19], which was later confirmed by X-ray crystallography [7]. As previously reported for α-helical structure, a shift to lower wavenumbers for β-sheet structure is obtained for MjNhaP1 as compared to NhaA, which also points to different intermolecular interaction in both proteins. The band absorbing at approx. 1627 cm^{-1} which we can reliably assign to intermolecular β-sheet points to the existence of MjNhaP1 as a protein in dimeric or trimeric form.

However, the main difference between the inactive and the active state of MjNhaP1 is found in a different content of ordered structural elements, which decreases with by increasing the pH-value. This high content of disordered structure in the inactive state is probably also the reason why Vinothkumar et al. could obtain 2D crystals at low pH and not at high pH values, which were poorly ordered tubes or small crystalline patches [8]. The high content of disordered structure of inactive protein at pD 8 was also supported by following the temperature-induced structural changes as well as by probing protein accessibility with H/D exchange.

The temperature profiles show a huge difference for α-helices between the inactive and the active state of MjNhaP1. While a melting temperature around 74 °C was observed at pD 6, half of the protein was already denaturated at 34 °C for pD 8. This finding of a decrease of the melting temperature by about 40 °C upon increasing the pD-value to pD 8 confirms the substantial structural differences in the region of α-helices between the inactive (pD 8) and the active (pD 6) protein. The unfolding process of this structure at pD 8 starts at a temperature about 25 °C lower as compared to the begin of the unfolding process of β-sheet structure at this protein state. In contrast to α-helical structure, almost no difference in the thermal stability was observed for β-sheet structure between the two states of the protein: the melting temperature was 62 °C at pD 6 and 58 °C at pD 8 for β-sheet structure.

These results demonstrate that thermal stability of β-sheet structures is not affected by the activation process of the protein. In the inactive state the instability of α-helical structure does not cause the change of β-sheet.

In the case of NhaA, the β-sheet builds a main contact between monomers [41–45]. Since the thermal stability of β-sheet structure is higher ($\Delta T_M = 25$ °C) than that of the α-helices in the inactive state of MjNhaP1, we assume that the function of β-sheet is the same or similar to the one found in NhaA. The increase of the melting temperature for the inactive state can be described as initiated by the unfolding of the instable α-helical region. After that, monomerization occurs.

In the active state, the melting point for that α-helical structure is approx. 10 °C higher than that for the β-sheet. Thus, monomerization does probably not lead to a loss of the antiporter function as in the case of NhaA [44,45].

The thermal instability of the protein in the inactive state at pD 8 is due to high amount of unordered structure, which was confirmed by H/D exchange experiments.

However, the highest temperature stability was observed for α-helices at pD 6 at 74 °C. This temperature is low considering that MjNhaP1 originates from a hyperthermophilic archeon-organism with unique lipids. The reason for this low temperature could be because of the investigation of the protein in DDM micelles. As observed by Sukumaran et al. the stability of the protein can be decreased when investigating the protein in detergent micelles in comparison to the protein in lipids [46]. But this decreased thermal stability of the protein in detergent micelles does not have to be in line with loss of the functionality of the protein. Rather because in case of MjNhaP1 although it originates from hyperthermophilic archeon with unique lipids, the recombinant protein could be expressed heterologously in *E. coli* and extracted from the *E. coli* membranes in DDM. The purified protein shows a homogeneous peak at pH 4.0 as analysed by gel filtration profile over several time points i.e. the protein is stable in DDM solution at room temperature after elution from the Nickel column up to 48 h. But the protein appears more stable at pH 4.0 than at pH 8.0 in gel filtration profiles. This purified protein yields well-ordered 2D crystals in *E. coli* polar lipids (Avanti), which were used to calculate a projection map. This projection map shows structural similarity to *E. coli* NhaA.

Also the analysis of MjNhaP1 by blue native gel electrophoresis functional experiment showed that the protein is functional in DDM [8].

The H/D experiments provided the information on the accessibility of protein backbone groups for functionally different states. Extrapolation of the data obtained up to ~400 min show that at pH/pD 6 approx. 29% and at pH/pD 8 approx. 58% of peptide groups of MjNhaP1 were exchanged. These results show that the accessible fraction of the polypeptide chain of MjNhaP1 increases by about 30% with increasing the pH/pD-value. This corresponds to 30% of the unordered structure found from the secondary structure analysis of the protein in the inactive state, which is easily accessible by the buffer solution. The remaining ~30% of exchanged peptide groups are proposed to be located in the loops which connect the transmembrane helical segments. The same extent of exchange rate is also observed for the active state at pH/pD 6.

As previously mentioned, the model deduced from the amino acid sequence proposed 13 transmembrane segments of the protein [6]. The hydrophilic region thus constitutes approx. 36% (154 aa) of the protein structure. At the end of H/D exchange experiment (after ~24 h), about 35% of peptide groups have been accessible for D_2O in the active state of the protein. This percentage probably represents the entire hydrophilic region and supports the folding in 13 transmembrane segments.

However, approx. 6% of these accessible peptide groups exchange relatively slowly. These slowly exchanging groups are only observed in the active state of the protein. They amount to approx. 26 peptide groups. It can be argued that this slowly exchanging component could be due to the peptide groups that are located in the hydrophobic core of the protein and hence will exchange slowly relative to the buffer-exposed regions of the protein [14,20,21,47]. This would implicate that the hydrophilic region accounts for 128 amino acids rather than 154 amino acids, corresponding to 14 transmembrane segments. Another argument could be that 6% of slowly exchanging peptide groups observed in the active state belongs to ordered structure elements like α-helix and β-sheet that are located in the hydrophilic region. Such ordered groups will exchange with D_2O much slower than the unordered structure or turns [12,20,32].

Altogether, the results obtained here from IR spectroscopy present an extremely ordered, thermally stable and hydrophobic active state of MjNhaP1. In contrast, the inactivation of the protein is accompanied by conformational changes resulting in more unordered conformation with decreased thermal stability and an increased accessible fraction of the polypeptide chain.

Acknowledgements

The authors would like to thank the Deutsche Forschungsgemeinschaft (SFB 472, P21) and the International Max-Planck-Research School for financial support.

References

[1] E. Padan, M. Venturi, Y. Gerchman, N. Dover, Na^+/H^+ antiporters, Biochim. Biophys. Acta 1505 (2000) 144–157.
[2] E. Padan, T. Tzubery, K. Herz, L. Kozachkov, A. Rimon, L. Galili, NhaA of *Escherichia coli*, as a model of a pH regulated Na^+/H^+ antiporter, Biochim. Biophys. Acta 1658 (2004) 2–13.
[3] E. Padan, E. Bibi, M. Ito, T.A. Krulwich, Alkaline pH homeostasis in bacteria: new insights, Biochim. Biophys. Acta 1717 (2005) 67–88.
[4] E. Padan, S. Schuldiner, Molecular physiology of the Na^+/H^+ antiporter in *Escherichia coli*, J. Exp. Biol. 196 (1994) 443–456.
[5] J. Hellmer, R. Pätzold, Identification of a pH regulated Na^+/H^+ antiporter of *Methanococcus jannaschii*, C. Zeilinger, FEBS Lett. 527 (2002) 245–249.
[6] J. Hellmer, A. Teubner, C. Zeilinger, Conserved arginine and aspartate residues are critical for function of MjNhaP1, a Na^+/H^+ antiporter of *M. jannaschii*, FEBS Lett. 542 (2003) 32–36.
[7] C. Hunte, E. Screpanti, M. Venturi, A. Rimon, E. Padan, H. Michel, Structure of Na^+/H^+ antiporter and insights into mechanism of action and regulation by pH, Nature 435 (2005) 1197–1202.
[8] K.R. Vinothkumar, S.H.J. Smits, W. Kühlbrandt, pH-induced structural change in a sodium/proton antiporter from *Methanococcus jannaschii*, EMBO J. 24 (2005) 2720–2729.
[9] E. Olkhova, C. Hunte, E. Screpanti, E. Padan, H. Michel, Multiconformation continuum electrostatics analysis of the NhaA Na^+/H^+ antiporter of *Escherichia coli* with functional implications, Proc. Natl. Acad. Sci. U. S. A. 103 (2006) 2629–2634.
[10] T. Arkin, H. Xu, M.O. Jensen, E. Arbely, E.R. Bennett, K.J. Bowers, E. Chow, R.O. Dror, M.P. Eastwood, R. Flitman-Tene, B.A. Gregersen, J.L. Klepeis, I. Kolossvary, Y. Shan, D.E. Shaw, Mechanism of Na^+/H^+ antiporting, Science 317 (2007) 799–803.
[11] H. Fabian, W. Mäntele, Infrared spectroscopy of proteins, Handb. Vibr. Spectrosc. 5 (2002) 3426–3452.
[12] A. Barth, Infrared spectroscopy of proteins, Biochim. Biophys. Acta 1767 (2007) 1073–1101.
[13] E. Goormaghtigh, V. Cabiaux, J.M. Ruysschaert, Determination of soluble and membrane protein structure by Fourier transform infrared spectroscopy III: Secondary structures, Subcell Biochem. 23 (1994) 405–450.
[14] J. Grdadolnik, Y. Maréchal, Hydrogen-deuterium exchange in bovine serum albumin protein monitored by fourier transform infrared spectroscopy, part I: Structural studies, Appl. Spectrosc. 59 (2005) 1347–1356.
[15] N.N. Kalnin, S.Y. Venyaminov, QuantitativeIR , Spectrophotometry of peptide compounds in water (H_2O) solutions. III. Estimation of the Protein Secondary Structure, Biopolym. 30 (2005) 1273–1280.
[16] J. Alvarez, D.C. Lee, S.A. Baldwin, D. Chapman, Fourier transform infrared spectroscopic study of the structure and conformational changes of the human erythrocyte glucose transporter, J. Biol. Chem. 262 (1987) 3502–3509.
[17] J.L.R. Arrondo, J. Castresana, J.M. Valpuesta, F.M. Goñi, Structure and thermal denaturation of crystalline and noncrystalline cytochrome oxidase as studied by infrared spectroscopy, Biochemistry 33 (1994) 11650–11655.
[18] C. Zscherp, H. Aygün, J.W. Engels, W. Mäntele, Effect of proline to alanine mutation on the thermal stability of the all-β-sheet protein tendamistat, Biochim. Biophys. Acta 1651 (2003) 139–145.
[19] E. Dzafic, O. Klein, E. Screpanti, C. Hunte, W. Mäntele, Flexibility and dynamics of NhaA Na^+/H^+-antiporter of *Escherichia coli* studied by Fourier transform infrared spectroscopy, Spectrochim. Acta A 72 (2009) 102–109.
[20] E. Goormaghtigh, V. Cabiaux, J.M. Ruysschaert, Determination of soluble and membrane protein structure by Fourier transform infrared spectroscopy II. Experimental aspects, side chain structure, and H/D exchange, Subcell Biochem. 23 (1994) 363–403.
[21] C. Vigano, M. Smeyers, V. Raussens, F. Scheirlinckx, J.M. Ruysschaert, Hydrogen–deuterium exchange in membrane proteins monitored by IR spectroscopy: a new tool to resolve protein structure and dynamics, Biopolymers 74 (2003) 19–26.
[22] J. Grdadolnik, Y. Maréchal, Hydrogen–deuterium exchange in bovine serum albumin protein monitored by Fourier transform infrared spectroscopy, part II: Kinetic studies, Appl. Spectrosc. 59 (2005) 1357–1364.
[23] F.W. Studier, Protein production by auto-induction in high density shaking cultures, Protein Expr. Purif. 41 (2005) 207–234.
[24] A.K. Covington, M. Paabo, R.A. Robinson, R.G. Bates, Use of the glass electrode in deuterium oxide and the relation between the standardized pD (paD) scale and the operational pH in heavy water, Anal. Chem. 40 (1968) 700–706.
[25] N. Dave, A. Troillier, I. Mus-Veteau, M. Duñach, G. Leblanc, E. Padros, Secondary structure components and properties of the melibiose permease from *Escherichia Coli*: a Fourier transform infrared spectroscopy analysis, Biopys. J. 79 (2000) 747–755.
[26] D.M. Byler, H. Susi, Examination of the secondary structure of proteins by deconvolved FTIR spectra, Biopolymers 25 (1986) 469–487.
[27] I. Iloro, R. ChehÍn, F.M. Goñi, M. Pajares, J.L.R. Arrondo, Methionine adenosyltransferase alpha-helix structure unfolds at lower temperatures than beta-sheet: a 2D-IR study, Biophys. J. 86 (2004) 3951–3958.
[28] T. Heimburg, D. Marsh, Investigation of secondary and tertiary structural changes of cytochrome *c* in complexes with anionic lipids using amide hydrogen exchange measurements: an FTIR study, Biophys. J. 65 (1993) 2408–2417.
[29] T. Miyazawa, Perturbation treatment of the characteristic vibrations of polypeptide chains in various configurations, J. Chem. Phys. 32 (1960) 1647–1652.
[30] P.W. Holloway, H.H. Mantsch, Structure of cytochrome b5 in solution by Fourier-transform infrared spectroscopy, Biochemistry 28 (1989) 931–935.
[31] W.C. Reisdorf, S. Krimm, Infrared amide I' band of the coiled coil, Biochemistry 35 (1996) 1383–1386.
[32] A. Barth, C. Zscherp, What vibrations tell us about proteins, Rev. Biophys. 35 (2002) 369–430.
[33] A. Barth, The infrared absorption of amino acid side chains, Biophys. Mol. Biol. 74 (2000) 141–173.
[34] L. Galili, A. Rothman, L. Kozachkov, A. Rimon, E. Padan, Trans membrane domain IV is involved in ion transport activity and pH regulation of the NhaA-Na^+/H^+ antiporter of *Escherichia coli*, Biochemistry 41 (2001) 609–617.
[35] M. Van de Weert, P.I. Haris, W. Hennink, D.J.A. Crommelin, Fourier transform infrared spectrometric analysis of protein conformation: effect of sampling method and stress factors, Biochemistry 297 (2001) 160–169.
[36] N. Speerama, R.W. Woody, On the analysis of membrane protein circular dichroism spectra, Protein Sci. 13 (2003) 100–112.
[37] V. Raussens, J.M. Ruysschaert, E. Goormaghtigh, Analysis of $^1H/^2H$ exchange kinetics using model infrared spectra, App. Spectrosc. 58 (2004) 68–82.
[38] H.H.J de Jongh, E. Goormaghtigh, J.M. Ruysschaert, Amide-proton exchange of water-soluble proteins of different structural classes studied at the submolecular level by infrared spectroscopy, Biochemistry 36 (1997) 13603–13610.
[39] J.S. Patzlaff, J.A. Moeller, B.A. Barry, R.J. Brooker, Fourier transform infrared analysis of purified lactose permease: a monodisperse lactose permease preparation is stably folded, alpha-helical, and highly accessible to deuterium exchange, Biochemistry 37 (1998) 15363–15375.
[40] J.L. Arrondo, F.M. Goñi, Structure and dynamics of membrane proteins as studied by infrared spectroscopy, Biophys. Mol. Biol. 72 (1999) 367–405.
[41] Y. Gerchman, A. Rimon, M. Venturi, E. Padan, Oligomerization of NhaA, the Na^+/H^+ antiporter of *Escherichia coli* in the membrane and its functional and structural consequences, Biochemistry 40 (2001) 3403–3412.
[42] D. Hilger, H. Jung, E. Padan, C. Wegener, K.P. Vogel, H.J. Steinhoff, G. Jeschke, Assessing oligomerization of membrane proteins by four-pulse DEER: pH-dependent dimerization of NhaA Na^+/H^+ antiporter of *E. coli*, Biophys. J. 89 (2005) 1328–1338.
[43] D. Hilger, Y. Polyhach, E. Padan, H. Jung, G. Jeschke, High-resolution structure of a Na^+/H^+ antiporter dimer obtained by pulsed electron paramagnetic resonance distance measurements, Biophys. J. 93 (2007) 3675–3683.
[44] RimonT. Tzubery , E. Padan, Monomers of the NhaA Na^+/H^+ antiporter of *Escherichia coli* are fully functional yet dimers are beneficial under extreme stress conditions at alkaline pH in the presence of Na^+ or Li^+, J. Biol. Chem. 282 (2007) 26810–26821.
[45] K. Herz, A. Rimon, G. Jeschke, E. Padan, {beta}-Sheet-dependent dimerization is essential for the stability of NhaA Na^+/H^+ antiporter, J. Biol. Chem. 284 (2009) 6337–6347.
[46] S. Sukumaran, K. Hauser, A. Rauscher, W. Mäntele, Thermal stability of outer membrane protein porin from *Paracoccus denitrificans*: FT-IR as a spectroscopic tool to study lipid–protein interaction, FEBS Lett. 579 (2005) 2546–2550.
[47] C. Vigano, E. Goormaghtigh, J.M. Ruysschaert, Detection of structural and functional asymmetries in *P-glycoprotein* by combining mutagenesis and H/D exchange measurements, Chem. Phys. Lipids 122 (2003) 121–135.